

Mobility of an axisymmetric particle near an elastic interface: Supporting Information

Abdallah Daddi-Moussa-Ider,^{1, a)} Maciej Lisicki,^{2, 3, a)} and Stephan Gekle¹

¹⁾*Biofluid Simulation and Modeling, Fachbereich Physik,
Universität Bayreuth, Universitätsstraße 30, Bayreuth 95440,
Germany*

²⁾*Institute of Theoretical Physics, Faculty of Physics,
University of Warsaw, Pasteura 5, 02-093 Warsaw,
Poland*

³⁾*Department of Applied Mathematics and Theoretical Physics,
Wilberforce Rd, Cambridge CB3 0WA, United Kingdom*

(Dated: 12 October 2016)

^{a)}ADMI and ML contributed equally to this work.

S1. VANISHING FREQUENCY LIMITS

In the following, we provide analytical expressions of the mobility corrections in the vanishing frequency limit. As mentioned in the main text, the corrections can conveniently be split up into a contribution due to shearing and a contribution due to bending.

A. Translational mobility

In the steady limit, i.e. when $\beta, \beta_B \rightarrow 0$, the correction to the mobility tensor near a hard-wall as calculated by Lisicki *et al.*¹ is recovered. From Eqs. (5.13)-(5.16), we obtain

$$\lim_{\beta, \beta_B \rightarrow 0} 8\pi\eta(2z_0)\Delta\mu^{tt} = -\frac{3}{2} \begin{pmatrix} 1 + \cos^2 \theta & 0 & -\sin \theta \cos \theta \\ 0 & 1 & 0 \\ -\sin \theta \cos \theta & 0 & 1 + \sin^2 \theta \end{pmatrix}. \quad (\text{S1})$$

The corrections due to shearing and bending in the vanishing frequency limit read

$$\lim_{\beta \rightarrow 0} 8\pi\eta(2z_0)\Delta\mu_S^{tt} = -\frac{1}{4} \begin{pmatrix} 5 - 3\cos^2 \theta & 0 & 3\sin \theta \cos \theta \\ 0 & 5 & 0 \\ 3\sin \theta \cos \theta & 0 & 5 - 3\sin^2 \theta \end{pmatrix}.$$

and

$$\lim_{\beta_B \rightarrow 0} 8\pi\eta(2z_0)\Delta\mu_B^{tt} = -\frac{1}{4} \begin{pmatrix} 1 + 9\cos^2 \theta & 0 & -9\sin \theta \cos \theta \\ 0 & 1 & 0 \\ -9\sin \theta \cos \theta & 0 & 1 + 9\sin^2 \theta \end{pmatrix},$$

which gives the hard-wall limit Eq. (S1) when summing up both parts.

B. Translation-rotation coupling

By taking the vanishing frequency limit in Eqs. (5.17)-(5.19) we obtain

$$\lim_{\beta, \beta_B \rightarrow 0} 8\pi\eta(2z_0)^2 \Delta\mu^{tr} = \frac{3\lambda}{2} \begin{pmatrix} 0 & \sin\theta(1 + \cos^2\theta) & 0 \\ 0 & 0 & \cos\theta \\ 0 & -\cos\theta(1 + \sin^2\theta) & 0 \end{pmatrix}. \quad (\text{S2})$$

The corrections due to shearing and bending in the vanishing frequency limit read

$$\lim_{\beta \rightarrow 0} 8\pi\eta(2z_0)^2 \Delta\mu_S^{tr} = \frac{3\lambda}{4} \begin{pmatrix} 0 & \sin^3\theta & 0 \\ 0 & 0 & \cos\theta \\ 0 & -\cos^3\theta & 0 \end{pmatrix}.$$

and

$$\lim_{\beta_B \rightarrow 0} 8\pi\eta(2z_0)^2 \Delta\mu_B^{tr} = \frac{3\lambda}{4} \begin{pmatrix} 0 & \sin\theta(1 + 3\cos^2\theta) & 0 \\ 0 & 0 & \cos\theta \\ 0 & -\cos\theta(1 + 3\sin^2\theta) & 0 \end{pmatrix},$$

which gives the hard-wall limit Eq. (S2) when summing up both parts.

C. Rotational mobility

From Eqs. (5.20)-(5.23), the corrections are found in the vanishing frequency limit to be

$$\lim_{\beta, \beta_B \rightarrow 0} 8\pi\eta(2z_0)^3 \Delta\mu_{11}^{rr} = -\frac{5}{2} + \frac{3}{2} \cos^2\theta, \quad (\text{S3a})$$

$$\lim_{\beta, \beta_B \rightarrow 0} 8\pi\eta(2z_0)^3 \Delta\mu_{13}^{rr} = -\frac{3}{2}(1 - \lambda) \sin\theta \cos\theta, \quad (\text{S3b})$$

$$\lim_{\beta, \beta_B \rightarrow 0} 8\pi\eta(2z_0)^3 \Delta\mu_{22}^{rr} = -\frac{9}{2}\lambda^2 - 3\lambda - \frac{5}{2} - \frac{3}{2}\lambda(\lambda - 4) \cos^2\theta + \frac{3}{2}\lambda^2 \cos^4\theta, \quad (\text{S3c})$$

$$\lim_{\beta, \beta_B \rightarrow 0} 8\pi\eta(2z_0)^3 \Delta\mu_{33}^{rr} = -1 - \frac{3}{2}\lambda^2 - \frac{3}{2}(2\lambda^2 - 2\lambda + 1) \cos^2\theta, \quad (\text{S3d})$$

in agreement with the results by Lisicki *et al.*¹.

In the vanishing frequency limit, the corrections due to shearing and bending are expressed for the component 11 as

$$\begin{aligned}\lim_{\beta \rightarrow 0} 8\pi\eta(2z_0)^3 \Delta\mu_{11,S}^{rr} &= -\frac{3}{2} + \frac{1}{2} \cos^2 \theta, \\ \lim_{\beta_B \rightarrow 0} 8\pi\eta(2z_0)^3 \Delta\mu_{11,B}^{rr} &= -\sin^2 \theta,\end{aligned}$$

leading to Eq. (S3a) after summing up both contributions.

For the component 13

$$\begin{aligned}\lim_{\beta \rightarrow 0} 8\pi\eta(2z_0)^3 \Delta\mu_{13,S}^{rr} &= -\frac{1}{2} \cos \theta \sin \theta, \\ \lim_{\beta_B \rightarrow 0} 8\pi\eta(2z_0)^3 \Delta\mu_{13,B}^{rr} &= -\left(1 - \frac{3\lambda}{2}\right) \sin \theta \cos \theta,\end{aligned}$$

which gives after summing up both contributions the result near a hard-wall Eq. (S3b).

For the component 22

$$\begin{aligned}\lim_{\beta \rightarrow 0} 8\pi\eta(2z_0)^3 \Delta\mu_{22,S}^{rr} &= -\frac{3}{2}(1 + \lambda^2) + \frac{3\lambda^2}{4} \cos^2 \theta - \frac{3}{4} \lambda^2 \cos^4 \theta, \\ \lim_{\beta_B \rightarrow 0} 8\pi\eta(2z_0)^3 \Delta\mu_{22,B}^{rr} &= -1 - 3\lambda(1 + \lambda) + 3\lambda \left(2 - \frac{3}{4}\lambda\right) \cos^2 \theta + \frac{9}{4} \lambda^2 \cos^2 \theta,\end{aligned}$$

leading to Eq. (S3c) when summing up both members.

For the component 33

$$\begin{aligned}\lim_{\beta \rightarrow 0} 8\pi\eta(2z_0)^3 \Delta\mu_{33,S}^{rr} &= -1 - \frac{3}{4} \lambda^2 - \left(\frac{1}{2} + \frac{3}{4} \lambda^2\right) \cos^2 \theta, \\ \lim_{\beta_B \rightarrow 0} 8\pi\eta(2z_0)^3 \Delta\mu_{33,B}^{rr} &= -\frac{3}{4} \lambda^2 - \left(1 - 3\lambda + \frac{9}{4} \lambda^2\right) \cos^2 \theta,\end{aligned}$$

which leads to Eq. (S3d) by summing up both contributions.

S2. CORRECTIONS IN THE LAB FRAME

The mobility corrections as considered in the main text are expressed in the particle frame. For the sake of completeness, we shall give in the following their expressions in the LAB frame $\{\mathbf{e}_x, \mathbf{e}_y, \mathbf{e}_z\}$.

A. Translational mobility

In the particle frame, the translational mobility corrections are stated by Eqs. (5.13)-(5.16). In the LAB frame, the tensor is diagonal and the corrections are expressed as

$$\begin{aligned} 8\pi\eta(2z_0)\Delta\mu_{11}^{tt} &= P, \\ 8\pi\eta(2z_0)\Delta\mu_{22}^{tt} &= P, \\ 8\pi\eta(2z_0)\Delta\mu_{33}^{tt} &= Q. \end{aligned}$$

B. Translation-rotation coupling

The translation-rotation coupling mobility corrections as given in the particle frame by Eqs. (5.17)-(5.19), are written in the LAB frame as

$$\begin{aligned} 8\pi\eta(2z_0)^2\Delta\mu_{12}^{tr} &= \lambda M(\beta, \beta_B)(1 - 2\cos^2\theta), \\ 8\pi\eta(2z_0)^2\Delta\mu_{21}^{tr} &= \lambda M(\beta, \beta_B)\cos^2\theta, \\ 8\pi\eta(2z_0)^2\Delta\mu_{23}^{tr} &= -\lambda M(\beta, \beta_B)\sin\theta\cos\theta, \\ 8\pi\eta(2z_0)^2\Delta\mu_{32}^{tr} &= \lambda(N(\beta, \beta_B) + 2M(\beta, \beta_B)\sin\theta\cos\theta). \end{aligned}$$

In the steady limit, we get

$$\lim_{\beta, \beta_B \rightarrow 0} 8\pi\eta(2z_0)^2 \Delta\mu^{tr} = \frac{3\lambda}{2} \begin{pmatrix} 0 & 1 - 2\cos^2\theta & 0 \\ \cos^2\theta & 0 & -\sin\theta\cos\theta \\ 0 & 3\sin\theta\cos\theta & 0 \end{pmatrix}.$$

C. Rotational mobility

The rotational mobility corrections as given in the particle frame by Eqs. (5.20)-(5.23), are written in the LAB frame as

$$\begin{aligned} 8\pi\eta(2z_0)^2 \Delta\mu_{11}^{rr} &= A_0 + (A_2 - A_0 + 2D + G_0) \cos^2\theta + (G_2 - A_2 - 2D) \cos^4\theta, \\ 8\pi\eta(2z_0)^2 \Delta\mu_{13}^{rr} &= (A_0 - D - G_0 + (A_2 + 2D - G_2) \cos^2\theta) \sin\theta\cos\theta, \\ 8\pi\eta(2z_0)^2 \Delta\mu_{33}^{rr} &= G_0 + (A_0 - 2D - G_0 + G_2) \cos^2\theta + (A_2 + 2D - G_2) \cos^4\theta, \end{aligned}$$

where the arguments β and β_B are dropped out for the sake of clarity. Note that the component 22 remains the same upon changing the frame of reference. In the vanishing frequency limit, we get

$$\begin{aligned} \lim_{\beta, \beta_B \rightarrow 0} 8\pi\eta(2z_0)^2 \Delta\mu_{11}^{rr} &= -\frac{5}{2} + \frac{3\lambda}{2}(2 - \lambda) \cos^2\theta - 3\lambda^2 \cos^4\theta, \\ \lim_{\beta, \beta_B \rightarrow 0} 8\pi\eta(2z_0)^2 \Delta\mu_{13}^{rr} &= \frac{3\lambda}{2} (\lambda(2 \cos^2\theta + 1) - 1) \cos\theta \sin\theta, \\ \lim_{\beta, \beta_B \rightarrow 0} 8\pi\eta(2z_0)^2 \Delta\mu_{33}^{rr} &= -1 - \frac{3\lambda^2}{2}(1 + \cos^2\theta) + 3\lambda^2 \cos^4\theta, \end{aligned}$$

S3. EFFECT OF THE INCLINATION ANGLE

In this section, we present the analytical predictions of the mobility corrections for an inclination angle of $\pi/6$. For the translational mobilities, we observe that the components 11 and 33 are predominately determined by bending and shearing respectively. This behavior is in contrast to that observed for $\pi/3$ presented in the main text.

We further observe that the coupling and rotational mobilities are primly determined for bending and shearing respectively, i.e. in the same way as obtained for $\theta = \pi/3$ reported in the main text.

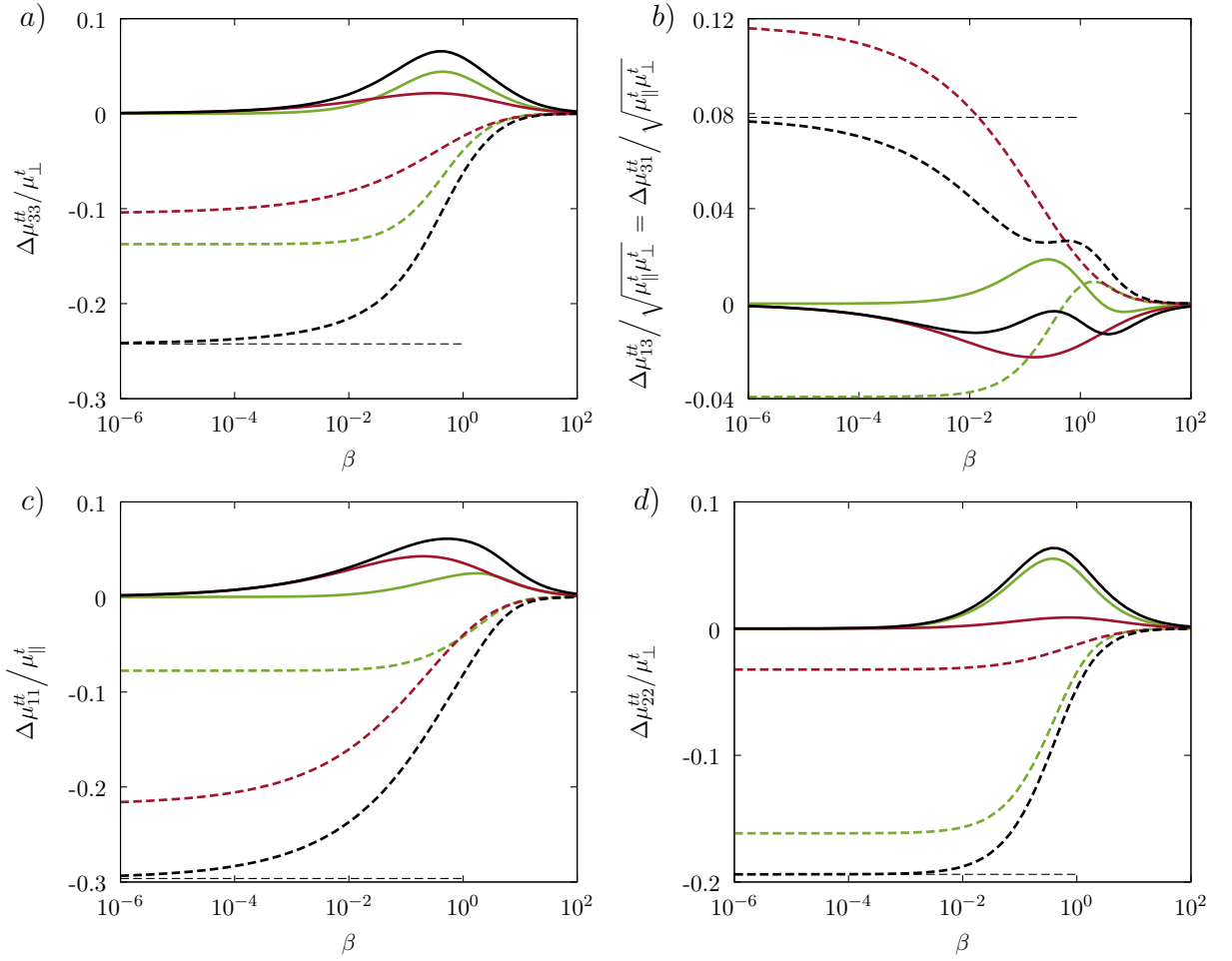


FIG. S1. (Color online) The scaled translational mobility correction components versus the scaled frequency using the same parameters of Fig. 2 of the main text with an angle $\theta = \pi/6$ from the vertical. The analytical predictions of the real and imaginary parts of the translational mobility corrections are shown as dashed and solid lines, respectively. The corrections due to shearing and bending are shown in green and red, respectively. Horizontal dashed lines represent the hard-wall limits.

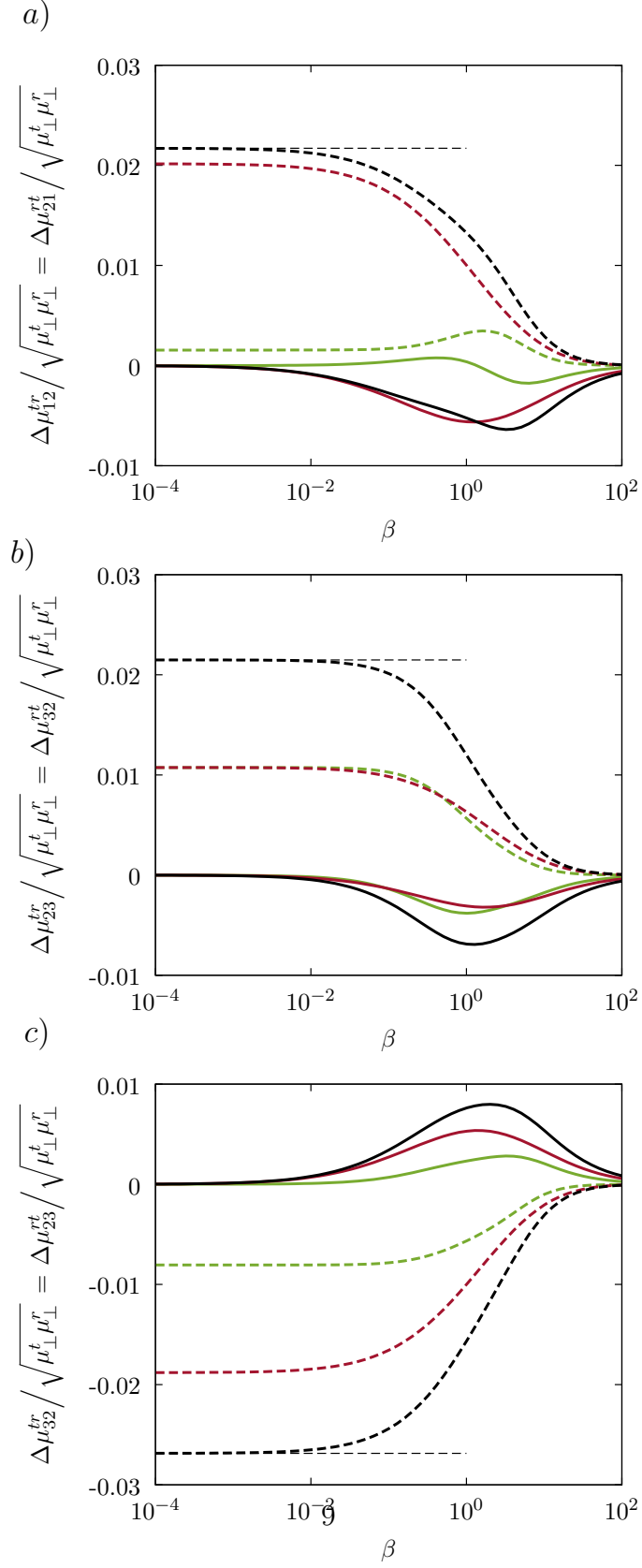


FIG. S2. (Color online) The scaled coupling mobility corrections versus the scaled frequency using the same parameters of Fig. 3 of the main text with an angle $\theta = \pi/6$ from the vertical.

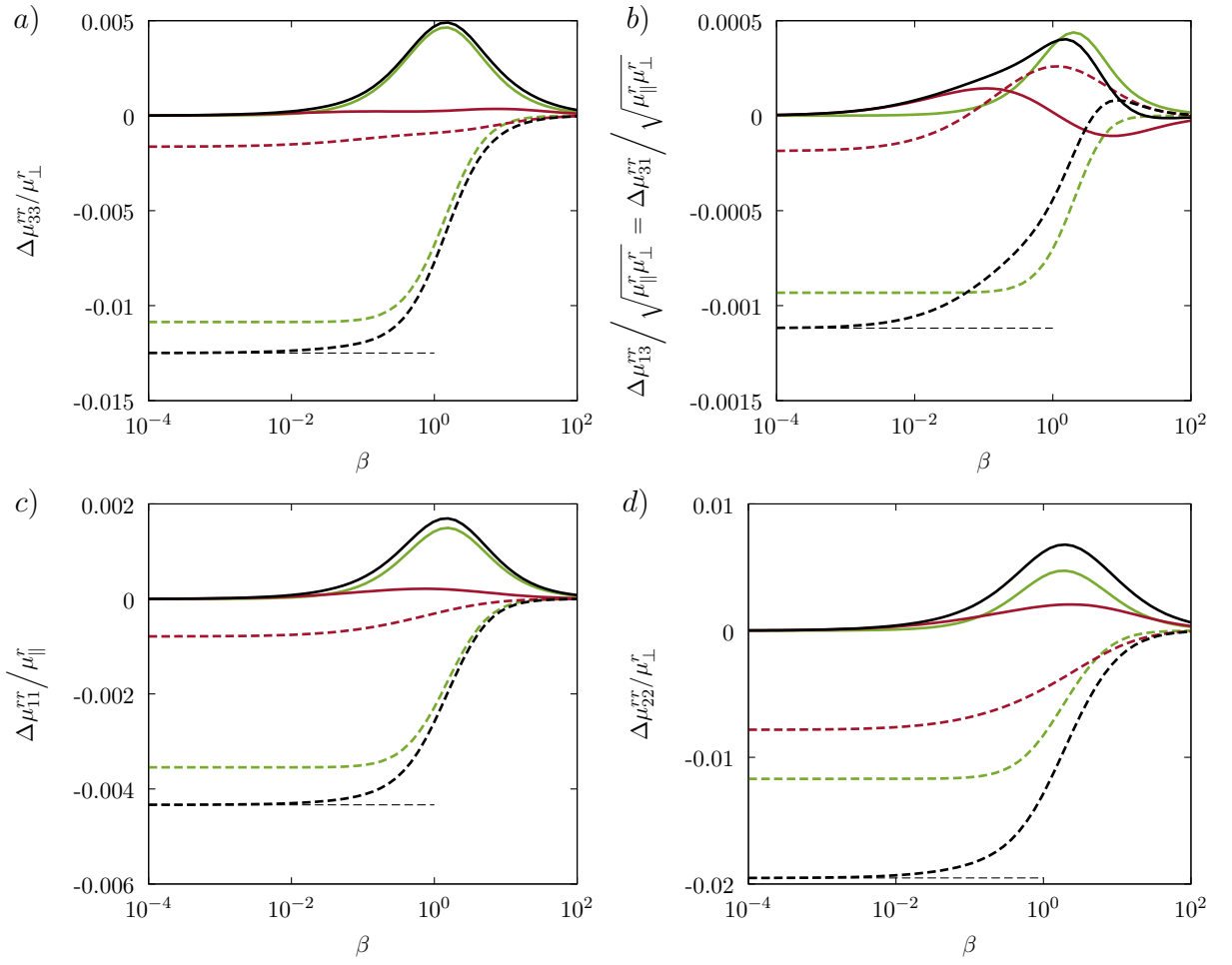


FIG. S3. (Color online) The scaled rotational mobility correction component versus the scaled frequency using the same parameters of Fig. 4 of the main text with an angle $\theta = \pi/6$ from the vertical.

S4. EFFECT OF REDUCED BENDING MODULUS

In this section, we present the analytical predictions of the mobility corrections using the same parameters of Fig. 2 with a reduced bending modulus 1000 times larger for which $\beta/\beta_B \sim 10^3$. We observe that the total mobility correction in the high frequency regime follows faithfully the bending related part in the mobility correction.

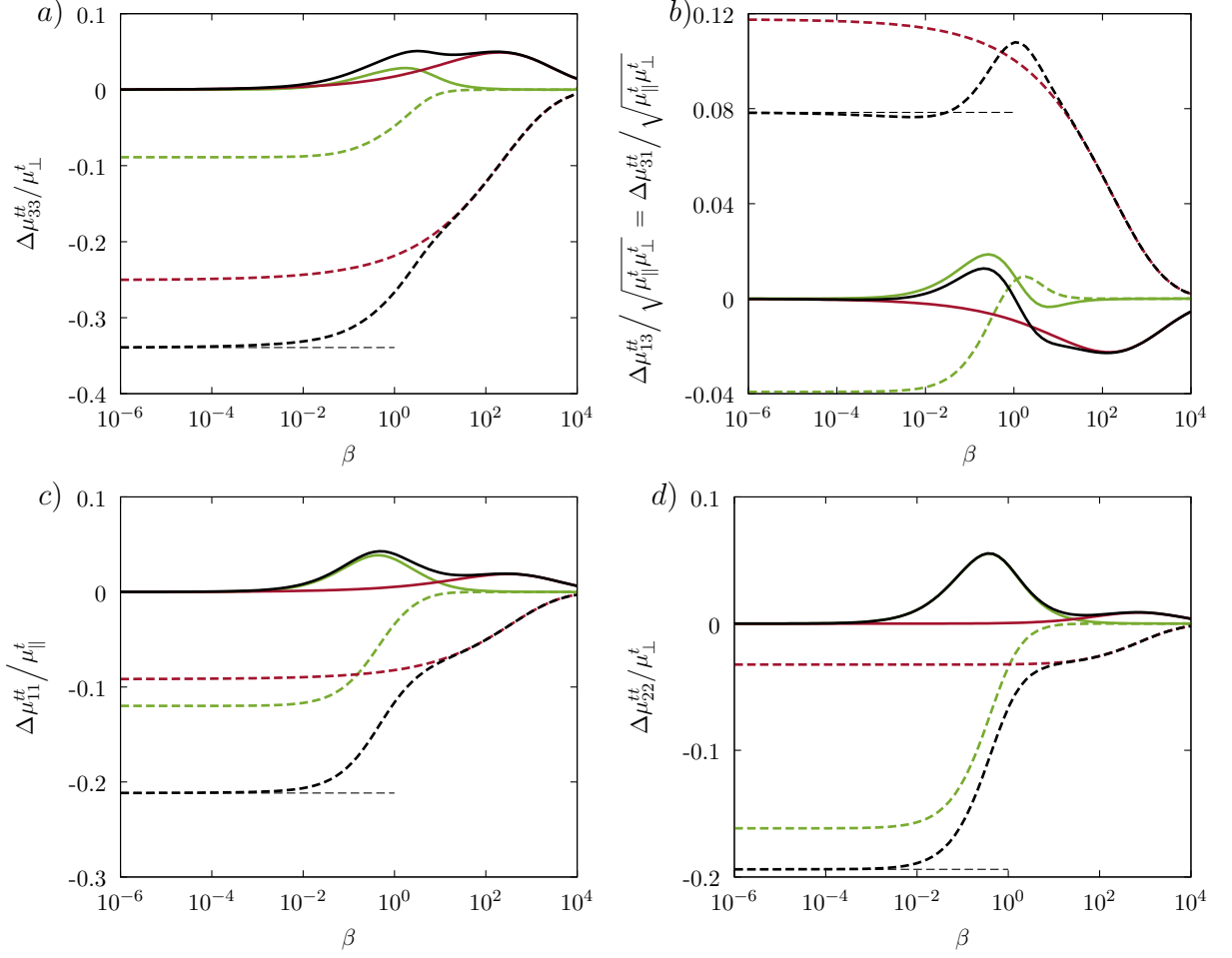


FIG. S4. (Color online) The scaled translational mobility correction components versus the scaled frequency using the same parameters of Fig. 2 of the main text with a reduced bending modulus 1000 times larger. The analytical predictions of the real and imaginary parts of the translational mobility corrections are shown as dashed and solid lines, respectively. The corrections due to shearing and bending are shown in green and red, respectively. Horizontal dashed lines represent the hard-wall limits.

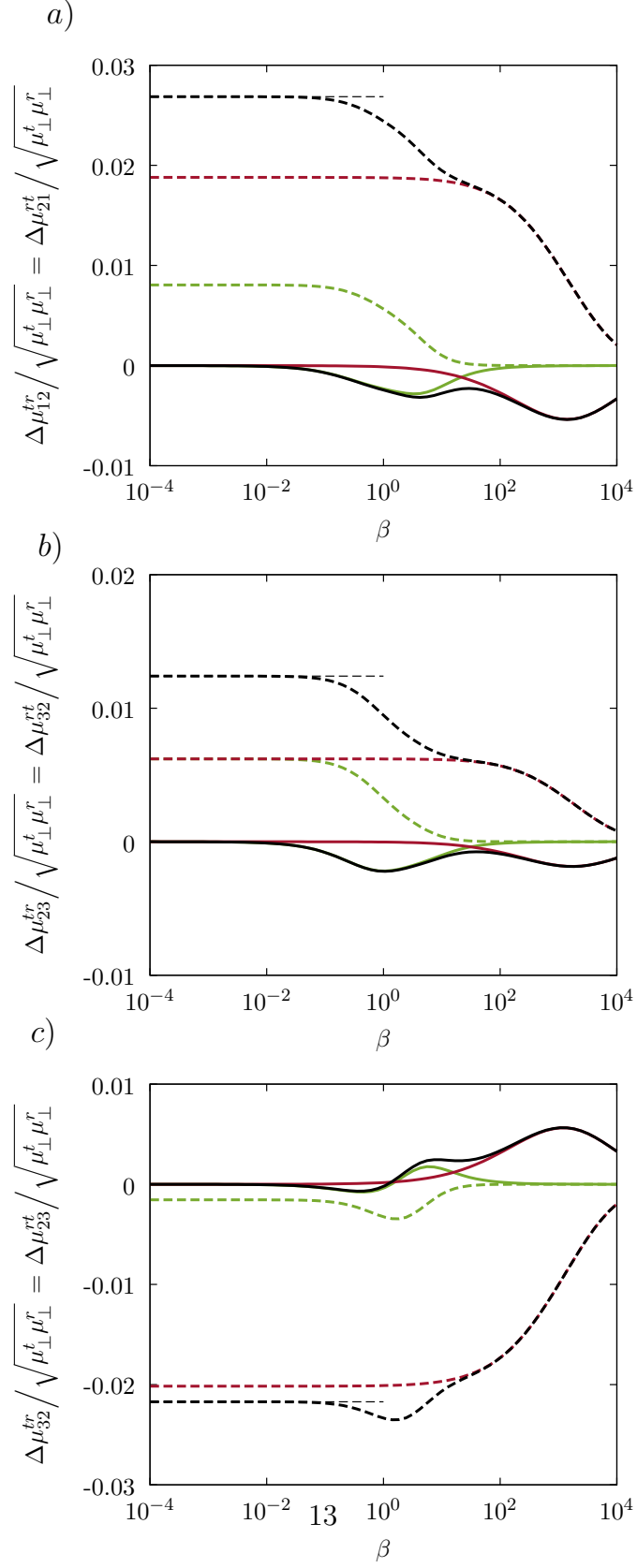


FIG. S5. (Color online) The scaled coupling mobility corrections versus the scaled frequency using the same parameters of Fig. 3 of the main text with a reduced bending modulus 1000 times larger.

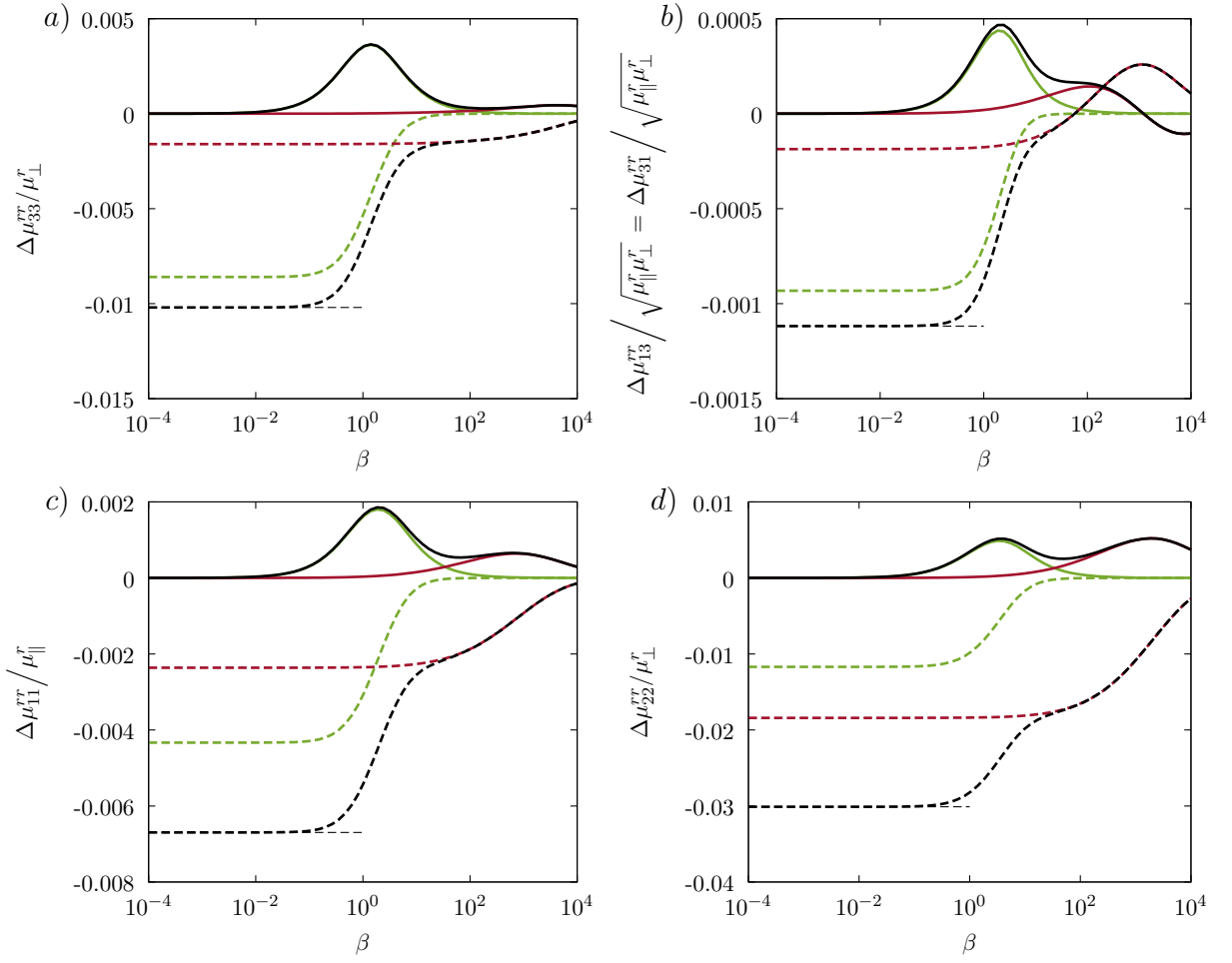


FIG. S6. (Color online) The scaled rotational mobility correction component versus the scaled frequency using the same parameters of Fig. 4 of the main text with a reduced bending modulus 1000 times larger.

REFERENCES

- ¹M. Lisicki. *Evanescent wave dynamic light scattering by optically anisotropic Brownian particles*. PhD thesis, University of Warsaw, 2015.